Coherence, ionization, and recombination in a microwave field

Vincent Carrat, E. Magnuson, and T. F. Gallagher
Department of Physics, University of Virginia, Charlottesville, Virginia 22904, USA
(Received 15 May 2015; published 16 December 2015)

An amplitude-modulated near-infrared laser pulse synchronized to a 14-GHz microwave field is used to excite atoms to the vicinity of the ionization limit at specific phases of the microwave field. When the laser is tuned above and below the ionization limit, phase-dependent modulation is observed in the recombination and ionization, respectively. The phase-dependent modulation is 10% of the total excitation, far greater than the 0.1% modulation observed with single-picosecond laser pulse excitation, and in agreement with calculations based on coherent excitation over several microwave cycles [Phys. Rev. Lett. **95**, 013001 (2005)].

DOI: 10.1103/PhysRevA.92.063414 PACS number(s): 32.80.Rm, 32.80.Ee, 32.80.Qk

I. INTRODUCTION

An extreme ultraviolet (XUV) attosecond pulse train (APT) phase synchronized with the strong infrared (IR) field from which it was generated provides a powerful tool for strong-field physics. The APT can be used to characterize the intense IR pulse, probe the response of an atom to the strong IR field on a subcycle timescale, and generate a richer variety of wave packets than is possible by using the intense IR pulse alone [1–5]. For example, ionization of an atom by a strong IR field favors ionization at the peak of the IR field, leading to the production of low-energy electrons. In contrast, ionization by the combined APT and IR fields can occur at any phase of the IR field, resulting in control of the final electron energy [3,5].

A beautiful example of the latter phenomenon is provided by the ionization of He by an XUV APT phase synchronized with a strong IR field [3,5]. In these experiments the central XUV photon energy is less than the ionization potential of He, and little ionization results from the APT alone. However, when He is exposed to both the APT and the IR field, ionization rates increase, and the rate depends on the phase of the IR field to which the APT is synchronized. The origin of the phase dependence is easily understood with a simple classical picture. The XUV pulse creates a photoelectron which departs from the He^+ core with insufficient energy to escape. The photoelectron is accelerated or decelerated by the IR field and thus gains or loses energy, depending on the phase of the IR field at which it was created. This picture is too simple in that it describes excitation by a single attosecond pulse, ignoring the coherence of the excitation by the APT [3]. Quantum-mechanical calculations indicate that the phase-dependent modulation of the ionization observed with excitation by a single attosecond pulse should be $\simeq$1%, not the 35% peak-to-peak modulation observed experimentally [3,6]. The much larger observed modulation is attributed to the coherent excitation of a wave packet by the APT over several IR field cycles.

In the He experiments the high-frequency field of the XUV APT produces a subthreshold photoelectron, and the low-frequency IR field transfers enough energy to the departing photoelectron that it can escape from the He^+ ion. The reverse process (i.e., the transfer of energy from the photoelectron to the low-frequency field) has also been observed, with a microwave field providing the strong low-frequency field and a visible laser providing the high-frequency field [7,8]. The visible laser photoionizes an atom, producing a free electron from which energy is removed by the microwave field, resulting in a bound atom [7]. A phase dependence analogous to that observed in the He experiments has been observed. Specifically, Li atoms photoionized by a 1-ps laser pulse in the presence of a phase-synchronized 17-GHz microwave field exhibit a phase-dependent modulation of the recombined bound atom signal [8]. However, the amplitude of the modulation is $\simeq$0.1% of the total excitation, far less than observed in the He experiments, but roughly consistent with the theoretical result for a single attosecond pulse [3].

Here we report the results of an experiment in which we have replaced the single-picosecond laser pulse with a laser beam which is amplitude modulated synchronously with a 14-GHz microwave field, so that laser excitation occurs over many microwave cycles. The use of an amplitude-modulated laser instead of a single ps pulse is analogous to replacing a single attosecond pulse by an APT. In addition, having only two frequency components, the amplitude-modulated beam brings out clearly the coherence in the laser excitation. By time delaying the laser beam we can alter the phase of the microwave field at which laser excitation occurs. When the laser is tuned over the ionization limit we see a large phase-dependent modulation in the recombination, $\simeq$10% of the total excitation, and with the laser tuned below the ionization limit we observe a similar phase-dependent modulation in the ionization. Thus, in the same system we are able to observe energy transfer from the photoelectron to the microwave field and vice versa. The dramatic increase in the observed phase-dependent modulation over that observed with the single ps laser pulse is due to the coherence of the laser excitation over several microwave cycles and the fact that the laser is tuned closer to the limit. In what follows we briefly review the classical model of energy transfer to or from the low-frequency field, describe the experimental approach, present the results, and discuss their implications.

II. CLASSICAL PICTURE

A one-dimensional classical picture of the energy transfer to or from the microwave field is shown in Fig. 1. Laser excitation produces photoelectrons in the energetic vicinity of the limit at time t_0, and they depart from the parent ion both to the left and right with velocity $\mathbf{v}(t_0)$, as shown. If the excitation occurs in the presence of a low-frequency field

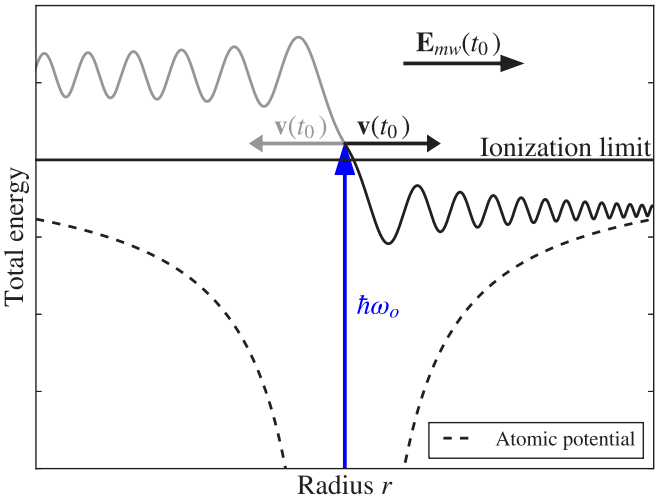

FIG. 1. (Color online) Laser excitation at time t_0 to an energy slightly above the ionization limit, shown by the vertical arrow, ejects electrons to the left and right with velocities $\pm v(t_0)$. The excitation occurs at the phase ωt_0 of the microwave field. The solid oscillatory lines show the electrons ejected to the right and left for $\omega t_0 = \pi/6$, when the instantaneous field is to the right, as shown. As electrons move away from the ion, there is a large energy exchange in the first half microwave cycle, and then the energy oscillates synchronously with the microwave field. While the average energy transfer up and down is the same for left and right going electrons, the oscillation amplitude and spatial period are larger for the former since they have higher velocity.

$\mathbf{E}_{mw}(t_0) = E_{mw}\cos\omega t_0$ instantaneously pointing to the right, as shown in Fig. 1, the field retards photoelectrons departing to the right and accelerates those departing to the left. If the laser is tuned above the limit, electrons ejected to the right can recombine, and on the subsequent half microwave cycle, electrons ejected to the left can recombine. As a result, we observe recombination twice in each microwave cycle. If a photoelectron is created at time t_0 the classical energy transfer W to the electron from the low frequency field $\mathbf{E}_{mw}(t)$ is given by [7]

$$W = -\int_{t_0}^{t} \mathbf{v}(t')\cdot\mathbf{E}_{mw}(t')dt', \tag{1}$$

where $\mathbf{v}(t)$ is the velocity of the photoelectron. Unless specified otherwise, we use atomic units. Unlike the simplest models of above threshold ionization (ATI) [9–11], the velocity does not come from the microwave field, but from the Coulomb field, assuming the microwave field to be relatively weak compared to the Coulomb field. In particular the microwave field is weak compared to the Coulomb field at small classical radius where the net energy transfer occurs, as shown in Fig. 1. As a result, for such fields the energy transfer is linear, not quadratic, in the field amplitude and far in excess of the ponderomotive energy, $U_P = E_{mw}^2/(4\omega^2)$. Here, ω is the angular frequency of the microwave field. For a photoelectron created near the limit, $v \simeq \sqrt{2/r}$, where r is the distance from the ion to the electron. Since the velocity decreases quickly as the electron leaves the ion, much of the energy transfer from a sinusoidal microwave field occurs during the first field cycle, and the phase of the microwave field at which excitation occurs is extremely important. If the microwave field is given by $E_{mw}(t) = E_{mw}\sin\omega t$ our calculations indicate that the maximum energy transfer occurs for the phases $\omega t_0 \simeq \pi/6$ and $7\pi/6$, with the magnitude of the energy transfer given by [7]

$$W_{\pi/6} \simeq \frac{3}{2}\frac{E_{mw}}{\omega^{2/3}}. \tag{2}$$

For $\omega/2\pi = 14$ GHz and $E_{mw} = 5$ V/cm, $W_{\pi/6} \simeq 40$ GHz, and $U_P = 360$ MHz. At $\omega t_0 \simeq \pi/6$ electrons departing to the right are maximally retarded, and those moving to the left are maximally accelerated. At $\omega t_0 \simeq 7\pi/6$ the roles are reversed. The implication of Eq. (2) is that to observe a bound atom subsequent to laser excitation above the limit, the laser must be tuned within $W_{\pi/6}$ of the ionization limit. Inversely, for a given laser detuning it gives the minimum required microwave amplitude.

The two trajectories plotted in Fig. 1 are computed by launching the electron initially at the center of a soft-core atomic potential [12,13] $V_a(r) = -[r^2 + (1/V_0^2)]^{-1/2}$ with $V_0 = 0.707$. The initial velocity is computed from the total energy of the system: $v(0) = \pm\sqrt{2(U_i + V_0)}$, with U_i being the laser detuning relative to the ionization limit. It is positive for the laser tuned over the limit and negative otherwise.

III. EXPERIMENTAL METHOD

A. General approach

In this experiment Li atoms in a beam pass through the central antinode of a 14 GHz Fabry–Perot microwave cavity where they are optically excited by the route $2s \xrightarrow{670\text{ nm}} 2p \xrightarrow{610\text{ nm}} 3d \xrightarrow{819\text{ nm, AM}} nf,\epsilon f$. The pulsed lasers driving the first two transitions propagate along the cavity axis. The third transition is driven by the amplitude-modulated 819-nm laser beam which crosses the other beams at a right angle at the center of the cavity, forming an excitation volume 1 mm on a side, a volume much smaller than the antinode's spatial extension. Thus, we consider the microwave field to be uniform over the excitation volume. Every field is linearly polarized along the vertical axis, allowing a one-dimensional treatment of the problem.

The microwave field is present in the cavity during the excitation and then shut off 10 ns after the end of the last laser pulse. One microsecond later we field ionize the surviving Rydberg atoms within 100 GHz ($n \gtrsim 180$) of the ionization limit by applying a negative voltage pulse to a plate below the cavity. The freed electrons travel through a hole in a plate above the cavity and are detected by a microchannel plate assembly (MCP). Electrons resulting from photoionization or microwave ionization have left the excitation volume by the time the field pulse is applied and are not detected. The MCP signal is integrated by a boxcar integrator and recorded by a computer for further analysis.

The essential idea of this experiment is shown in Fig. 2. The 819-nm laser is amplitude modulated synchronously with the microwave field present in the cavity. On the bottom of Fig. 2 we show the envelope of the 819-nm laser field; this field is

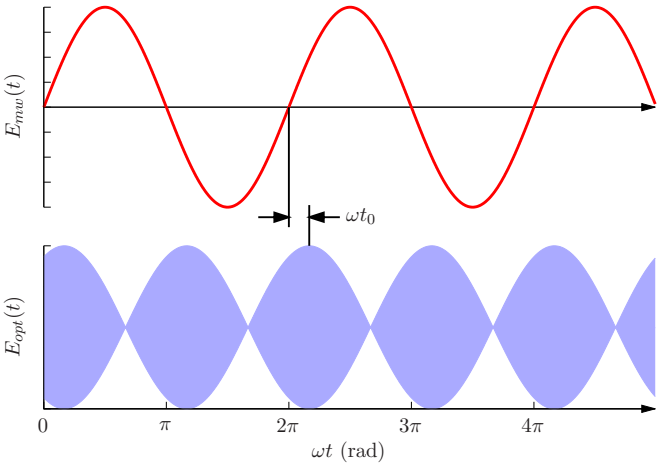

FIG. 2. (Color online) Temporal view of the microwave field (top) phase locked with the amplitude-modulated laser field $E_{\rm opt}$ (bottom). The maximum optical field occurs at the microwave phase ωt_0, and it is varied by using an optical delay line. In the figure, $\omega t_0 = \pi/6$, approximately the phase at which maximum energy transfer occurs.

given by

$$E_{\rm opt}(t) = E_o \sin(\omega_o t)\cos[\omega(t - t_0)]. \quad (3)$$

While we show the envelope of the laser field in Fig. 2, it is important to bear in mind that the probability of laser excitation is proportional to the laser intensity, the envelope of which has a $\cos^2[\omega(t - t_0)]$ dependence. The full width at half maximum of an intensity pulse is one quarter of the microwave period. In the He experiment the width of a single attosecond pulse was 370 as, one seventh of the IR period [3]. Besides the downscaling in frequency, this minor timing difference is the only difference between this experiment and the attosecond case.

By delaying the laser beam with an optical delay line we move the envelope of the optical field relative to the microwave field, altering the phase ωt_0 of the microwave field at which excitation occurs. We record the field ionization signal from Rydberg states as a function of the optical delay t_0, or equivalently the phase ωt_0 at which excitation occurs. In the following sections we describe the first two lasers used in the excitation, the production of the amplitude-modulated 819-nm beam, and the generation of the phase-locked microwave field.

B. Dye lasers

The 670-nm and 610-nm lasers are home-made pulsed dye lasers pumped by the 527 nm output of a Quantronix Nd:YLF laser running at a 1 kHz repetition rate. Each 200-ns-long pump pulse is sliced by using Pockels cells to produce 20-ns pulses in a setup similar to that of Ref. [14]. The first pulse is equally divided to pump the two dye lasers, and the second pulse pumps a dye amplifier for the 819 nm laser. The 670-nm laser is a Littman-type cavity [15] using LDS 698 dye in ethanol, while the 610-nm laser is a Hänsch-type cavity [16] with rhodamine 610 dye in ethanol. Before entering the microwave cavity those two 20-ns-long laser pulses are attenuated to 2 μJ by using optical density filters to avoid direct ionization, especially two 610-nm photon ionization from the $2p$ state.

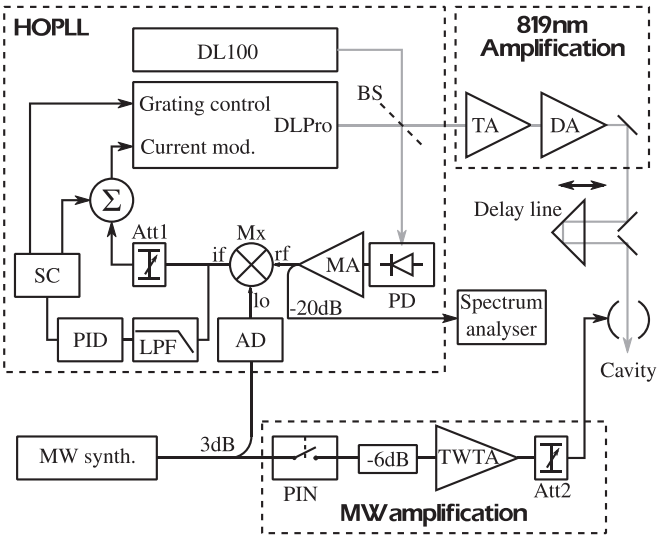

FIG. 3. Scheme of the experimental apparatus encompassing three different functions: generating the amplitude-modulated IR excitation laser, generating the microwave field, and phase locking the envelope of the 819-nm field to the microwave field as shown in Fig. 2. The 819-nm AMlaser is generated by the DL Pro and DL 100 lasers superimposed on the beam splitter (BS), and then amplified by the IR amplification chain. The microwaves are generated by a microwave synthesizer, formed into pulses by the PIN-diode switch (PIN) and amplified by the traveling-wave tube amplifier (TWTA) before injection in the cavity. The locking of the 819 nm field envelope to the microwave field is performed a heterodyne optical phase-locked loop (HOPLL).

C. Amplitude-modulated 819-nm laser

Figure 3 shows the production of the amplitude-modulated 819-nm laser beam and the detection of the amplitude modulation to phase lock the microwave field to the amplitude modulation. In the following paragraphs the labels in parentheses following each piece of equipment refer to the labels in Fig. 3.

We generate the 819-nm beam with 100% amplitude modulation by combining the outputs of two extended cavity diode lasers spaced in frequency by twice the 14-GHz microwave frequency. Specifically, the two lasers, a Toptica DL 100 (DL 100) and a Toptica DL Pro (DL Pro), are adjusted to have the same power and are superimposed on a 50 : 50 beamsplitter (BS). There are two 15-mW outputs from the beamsplitter. The first seeds the 819-nm amplification chain. It is amplified to 800 mW by the tapered amplifier (TA) and further amplified by the pulsed dye amplifier (DA). In the dye amplifier we use LDS 819 in ethanol. Ultimately we obtain 20-ns-long 6-μJ pulses which are sent to the microwave cavity after passing through an optical delay line. We checked that the pulse does not saturate the transition. The pulse amplification degrades the linewidth of the 819-nm lasers to about 100 MHz. The frequency spectrum of the pulse-amplified amplitude-modulated 819-nm laser beam is composed of two 100-MHz-wide peaks separated by 28 GHz.

The second output of the 50 : 50 beam splitter is sent to a fast (25 GHz bandwidth) photodiode (PD), which detects the 28-GHz-beat note. To phase lock the laser beat note on the second harmonic of the microwave field we use a heterodyne optical phase-locked loop (HOPLL). The beat signal is amplified by the low-noise amplifier (MA) and mixed with the second harmonic of the microwave oscillator by using a mixer (Mx). The intermediate frequency (if) output of the mixer is the error signal used in a dual phase lock loop correction scheme.

The high-frequency loop generates a fast proportional correction. In this loop the error signal is directly sent to the current modulation input of the DL Pro, with an attenuator (Att1) to adjust the correction gain. The bandwidth of the correction is most likely limited by the current modulation characteristics of the diode. Keeping the length of this loop as short as possible provides the most robust lock. Using solely this loop, the system stays locked typically for dozens of seconds, which is too short for performing our measurements. The loop loses lock because of the slow drift in the frequency difference between the two diode lasers. The frequency correction allowed by current modulation is limited to several megahertz to avoid mode hops, so when the difference frequency between the two lasers drifts more than a few megahertz from twice the microwave frequency, the lock is lost. The most important source of drift is the master oscillator, the DL 100: it is free running and consequently drifts over a few megahertz on a timescale of minutes.

To extend the locking time we added a low-frequency loop to correct for the slow drift of the DL 100 frequency. To implement the low frequency loop the error signal is sent through a 120-kHz low-pass filter (LPF) to a Toptica PID110 control module (PID). Through the Toptica SC110 scan control (SC) the PID 110 acts on both the diode current and the piezo controlling the grating angle. The grating angle correction is slow but can follow DL 100 drifts of hundreds of megahertz without causing mode hops. With those two loops working together we maintain continuous stable locks for several hours, greatly exceeding the 20 minutes needed to collect one data set. We used the dual-loop approach because the 8-kHz bandwidth of the Toptica PID 110 is not adequate.

Figure 4 shows spectra of the beat note before the mixer. In the bottom panel is shown the spectrum acquired in the free-running case. On a one-second timescale it shows a width of a few megahertz. The center frequency of this spectrum drifts by several megahertz on a 10-s timescale due to the drift in the frequency of the DL 100. The spectrum in the top panel is the beat-note spectrum obtained with the phase-lock loop turned on. It exhibits a strong and narrow peak at twice the microwave frequency ($2f_{mw}$), clearly showing that the system is locked. This central peak remains at the locking frequency as long as the system is locked. The two shoulders indicate a servo loop bandwidth of about 1 MHz. The central peak is 46 dB above the noise, as shown, and contains more than 99% of the power. The −20 dB bandwidth of the central peak is below 2 kHz; this measurement being limited by the 1-kHz resolution bandwidth (RBW) of our microwave spectrum analyzer. The overall performance of this system is sufficient for our use. Locking is routinely achieved in one or two minutes and requires little maintenance.

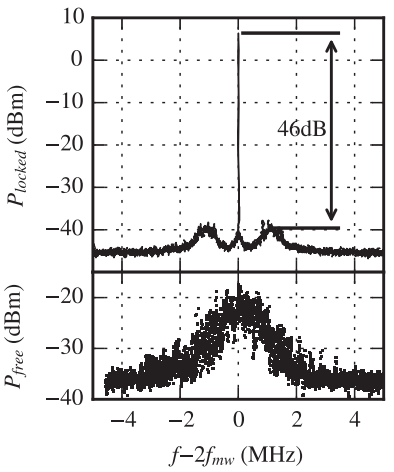

FIG. 4. Spectra of the laser beat note acquired by the spectrum analyzer shown in Fig. 3. The frequency is offset by twice the microwave frequency $2f_{mw}$. (top) Laser beat signal locked at $2f_{mw} =$ 28 GHz (RBW: 1 kHz, no averaging). (bottom) Beat-note spectrum when the lasers are free running (RBW: 10 kHz, no averaging).

D. Microwave apparatus

The microwave apparatus used is depicted on the bottom of Fig. 3. The microwave source is a Hittite HMC T-2100 synthesizer tuned to the 14.007-GHz resonance of the cavity. Using a 3-dB power splitter, half of its 11-dBm continuous wave (cw) output is frequency doubled by using the active doubler (AD) and used for the phase-locked loop described above. The remainder is formed into 300-ns-long pulses by using the PIN-diode switch (PIN) and amplified by a Hughes 8020H04F traveling wave tube amplifier (TWTA). Before the cavity a variable attenuator (Att2) is used to adjust the microwave power injected into the cavity. The Fabry–Perot cavity is composed of two brass mirrors, each with a 10 cm radius of curvature and a 10.2 cm diameter, with a 7.85 cm on axis separation. Operated on the TEM_{007} mode, it has a quality factor Q of 3700, and we are able to determine the field in the cavity with an uncertainty of 15%. A crucial aspect of the experiment is the reduction of stray electric fields, which ionize the high-lying states we detect [17]. To minimize stray fields, in addition to the plates above and below the cavity, we installed metal plates on both sides as well. Bias voltages are applied to the plates and the cavity mirrors to reduce the stray fields to 1.5 mV/cm, estimated by using the method described in Ref. [14].

The control of stray fields is more critical for low microwave frequencies [18], so we chose the highest frequency allowed by the bandwidth of the photodiode used in the locking system. To minimize stray fields we measure the field-dependent depression of the ionization limit by scanning one of the 819-nm lasers. The laser cannot be tuned further above the limit than its ≃30 GHz mode-hop free tuning range, and its tuning determines the minimum microwave field amplitude required to observe bound atoms subsequent to the microwave pulse. Specifically the minimum microwave field is given by Eq. (2) ($E_{mw} \simeq 2.5$ V/cm for 30 GHz above the limit). Microwave fields far in excess of this value lead to a decreased signal, as shown in Fig. 6.

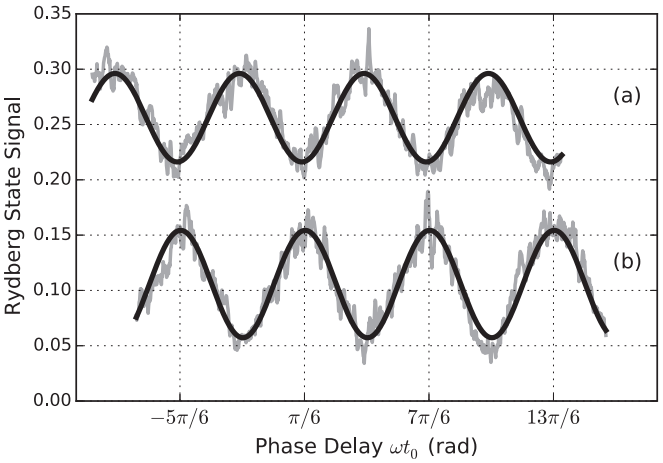

FIG. 5. Rydberg-state signal as a function of phase ωt_0 between the microwave field and laser envelope for two different laser tunings: (a) $\omega_0/2\pi$ is 17 GHz below the ionization limit, (b) $\omega_0/2\pi$ is 25 GHz above the limit. In both cases the microwave field is $E_{mw} = 3$ V/cm. The data (light gray) are fit to a sine function (black) to extract the peak-to-peak modulation. The total number of excited atoms in nf or ϵf states is 1.00 on this scale. The phase origin for the horizontal scale is chosen to have the maximum energy transfer up and down at $\pi/6$, in accordance with the results of our classical calculation. We observed that the two fits are inverted within 0.3 radian.

IV. RESULTS

In Fig. 5 we show result of tuning the amplitude-modulated 819-nm laser above and below the ionization limit. In both cases the Rydberg states are detected while scanning the optical delay as shown in Fig. 2. The vertical scale of the figure is relative to the total population promoted by the laser to nf or ϵf states. In Fig. 5(b) the center frequency $\omega_o/2\pi$ of the 819-nm laser is 25 GHz above the ionization limit, which is depressed by 7 GHz from its zero field value by the stray electric field. We see a large, 10%, phase-dependent modulation in the Rydberg state (recombination) signal. In Fig. 5(a) $\omega_o/2\pi$ is tuned 17 GHz below the ionization limit, and the observed signal is inverted from that shown in Fig. 5(b). Since we are detecting Rydberg states, the inverted signal indicates that with the laser tuned below the limit ionization occurs at the same phase ωt_0 as does recombination with the laser tuned above the limit, as expected from the classical model. Figure 5 shows two important features. First, we observe both energy transfer to the electron, as in the He experiments, and from the electron, as in the ps-microwave experiment. Second, the magnitude of the phase modulation, $\simeq$10%, is far greater than that observed with single ps laser pulse excitation.

In Fig. 6 we plot the observed modulation amplitudes for the tunings of Fig. 6 vs the microwave field as well as those calculated by using a classical model. The modulation in Fig. 6(a) is plotted as negative to indicate the phase reversal shown in Fig. 5. In Fig. 6(b), with the laser tuned above the limit, the experimental modulation signal increases to a maximum at $E_{mw} = 2.5$ V/cm and decreases to zero at 5 V/cm. In Fig. 6(a) the signal again increases to a maximum at 3 V/cm but, unlike in Fig. 6(b), slowly decreases as the field is raised, never reaching zero.

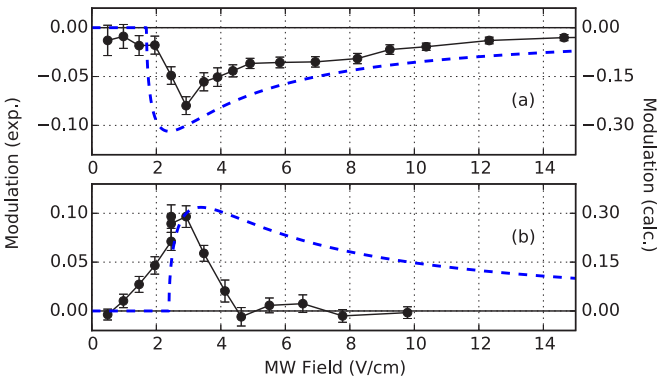

FIG. 6. (Color online) Peak-to-peak modulation of the Rydberg-state signal as a function of microwave field E_{mw} when the laser is tuned (a) 17 GHz below and (b) 25 GHz above the ionization limit. The experimental data points have error bars and the results of a classical calculation are shown as broken lines. The negative modulation in (a) reflects the phase inversion between Figs. 5(a) and 5(b). Note the factor-of-three difference in the two vertical scales.

It is instructive to compare the observed dependence of the modulation on the microwave field to the results of a one-dimensional classical model. In the model an electron near the ionization limit is launched from the center of a soft-core Coulomb potential at the phase ωt_0 of the microwave field [19]. We calculate numerically the classical motion of the electron to find the phase-dependent probability of its returning to the ionic core on its first orbit, ignoring later orbits. Since the Coulomb potential, not the microwave field, reflects the electron, it returns to the core with a negative total energy. It is worth noting that we calculate the motion of an electron within only one orbit but, as illustrated in Fig. 1, this orbit occurs over multiple microwave cycles. Furthermore, the Kepler frequency of a electron bound by 17 GHz is 500 MHz which is much lower than the microwave frequency. To avoid confusion, in the following "orbit" refers to the electronic motion whereas "cycle" refers to the microwave field. In Fig. 6(b) the laser tuning in the model is 25 GHz above the limit. There is no recombination until its onset at $E_{mw} = 2.5$ V/cm, when the maximum energy transfer of Eq. (2) equals the laser tuning above the limit. At this field, recombination occurs only at the phases $\omega t_0 \simeq \pi/6$ and $7\pi/6$. As the field is raised, recombination occurs over a widening phase interval, and the maximum modulation occurs when recombination occurs over the phase intervals $\pi/6 - \pi/4 \lesssim \omega t_0 \lesssim \pi/6 + \pi/4$ and $7\pi/6 - \pi/4 \lesssim \omega t_0 \lesssim 7\pi/6 + \pi/4$, which is, not surprisingly, when recombination occurs half the time. In Fig. 6(b) this occurs at $E_{mw} = 3$ V/cm. As E_{mw} is further increased the fraction of time during which recombination occurs increases, and the modulation slowly decreases. The calculated modulation shown in Fig. 6(a) is essentially the same.

V. DISCUSSION

The classical model provides useful insights into the experimental data. First, we note that, at fields above 3 V/cm, the model predicts a slow decrease in the modulation, which is observed in Fig. 6(a), but not in Fig. 6(b). It is not observed in Fig. 6(b) because an electron which has been recombined on

the first orbit, the only orbit considered in the model, can be ionized on a subsequent orbit, obliterating the modulation. In contrast, in Fig. 4(a) an electron ionized on the first orbit remains ionized; there are never any subsequent orbits. Thus Fig. 6(a) can be expected to match reasonably well a single-orbit model and, aside from the overall scale factor, it does. The discrepancy between the model and the experimental results in Fig. 6(b) at fields above 3 V/cm is evidently due to ignoring later orbits, when ionization can reduce the number of Rydberg states remaining to be detected.

There are two differences between the model and the experiment at low microwave fields. First, in both Figs. 6(a) and 6(b) the experimentally observed modulation rises more slowly than does the calculated modulation. Second, in Fig. 6(b) the onset of the modulation occurs before it is classically allowed; one of the hallmarks of a quantum mechanical process. While tunneling is the most familiar of such processes, a resonant transition driven by multiple field cycles is another [20].

The notion that multiple field cycles are important is the motivation for Floquet approaches to this and similar problems [6,21–23]. Further support for a Floquet approach comes from frequency domain experiments, in which series of peaks above the limit, separated by the microwave frequency, were observed [7,14,18], as well as from the phase dependence reported here. Since the amplitude-modulated laser field has only two optical frequency components, the relation between the relative phases of the two optical components at $\omega_0 \pm \omega$ and the phase of the envelope is particularly simple. A phase shift of ωt_0 in one of the components shifts the envelope by $\omega t_0/2$. Delaying the envelope is equivalent to shifting the phase of one of the two components. The observed phase dependence in Figs. 5 and 6 is thus indicative of coherent excitation of Floquet sidebands at $\omega_o \pm \omega$, as suggested previously [6].

While the classical one-orbit model is intuitively appealing, it overestimates the amplitude of the modulation by at least a factor of three, as shown by Fig. 6. We attribute this discrepancy to two factors: First, small, 1.5-mV/cm stray fields field ionize the high-lying states, reducing the size of all signals. Second, the model ignores the effect of later microwave cycles, which lead to more ionization, reducing the total detected signal, and the modulation as well.

VI. CONCLUSION

In conclusion, the enormous increase in the phase-dependent modulation signal when the laser excitation occurs over multiple microwave cycles, as opposed to during a single cycle [8], demonstrates experimentally the importance of coherence in the excitation, as predicted in He APT-IR laser calculations [3]. Furthermore, the energy transfer is much larger than expected on the basis of the microwave field alone, due to the presence of the Coulomb potential. For the same reason, in APT-IR experiments analogous energy transfer effects will be important even in relatively weak IR fields.

ACKNOWLEDGMENTS

It is a pleasure to acknowledge useful discussions with R.R. Jones. This work has been supported by the US Department of Energy (USA), office of Basic Energy Sciences, Chemical Sciences, Geosciences and Biosciences Division, under grant DE-FG02-97ER14786.

[1] E. Goulielmakis, M. Uiberacker, R. Kienberger, A. Baltuska, V. Yakovlev, A. Scrinzi, T. Westerwalbesloh, U. Kleineberg, U. Heinzmann, M. Drescher, and F. Krausz, Science **305**, 1267 (2004).

[2] N. Shivaram, H. Timmers, X.-M. Tong, and A. Sandhu, Phys. Rev. Lett. **108**, 193002 (2012).

[3] P. Johnsson, R. López-Martens, S. Kazamias, J. Mauritsson, C. Valentin, T. Remetter, K. Varjú, M. B. Gaarde, Y. Mairesse, H. Wabnitz, P. Salières, P. Balcou, K. J. Schafer, and A. L'Huillier, Phys. Rev. Lett. **95**, 013001 (2005).

[4] M. Chini, B. Zhao, H. Wang, Y. Cheng, S. X. Hu, and Z. Chang, Phys. Rev. Lett. **109**, 073601 (2012).

[5] P. Ranitovic, X. M. Tong, B. Gramkow, S. De, B. DePaola, K. P. Singh, W. Cao, M. Magrakvelidze, D. Ray, I. Bocharova, H. Mashiko, A. Sandhu, E. Gagnon, M. M. Murnane, H. Kapteyn, I. Litvinyuk, and C. L. Cocke, New J. Phys. **12**, 013008 (2010).

[6] X. M. Tong, P. Ranitovic, C. L. Cocke, and N. Toshima, Phys. Rev. A **81**, 021404 (2010).

[7] E. S. Shuman, R. R. Jones, and T. F. Gallagher, Phys. Rev. Lett. **101**, 263001 (2008).

[8] K. R. Overstreet, R. R. Jones, and T. F. Gallagher, Phys. Rev. Lett. **106**, 033002 (2011).

[9] H. van Linden van den Heuvell and H. Muller, *Multiphoton Processes* (Oxford University Press, Oxford, 2004).

[10] T. F. Gallagher, Phys. Rev. Lett. **61**, 2304 (1988).

[11] P. B. Corkum, N. H. Burnett, and F. Brunel, Phys. Rev. Lett. **62**, 1259 (1989).

[12] J. A. Hostetter, J. L. Tate, K. J. Schafer, and M. B. Gaarde, Phys. Rev. A **82**, 023401 (2010).

[13] J. Javanainen, J. H. Eberly, and Q. Su, Phys. Rev. A **38**, 3430 (1988). .

[14] J. H. Gurian, K. R. Overstreet, H. Maeda, and T. F. Gallagher, Phys. Rev. A **82**, 043415 (2010).

[15] M. G. Littman and H. J. Metcalf, Appl. Opt. **17**, 2224 (1978).

[16] T. W. Hänsch, Appl. Opt. **11**, 895 (1972).

[17] W. Zhao, J. C. Lancaster, F. B. Dunning, C. O. Reinhold, and J. Burgdörfer, J. Phys. B: At., Mol. Opt. Phys. **38**, S191 (2005).

[18] A. Arakelyan, T. Topcu, F. Robicheaux, and T. F. Gallagher, Phys. Rev. A **90**, 013413 (2014).

[19] J. H. Eberly, R. Grobe, C. K. Law, and Q. Su, *Atoms in Intense Laser Fields*, edited by M. Gavrila (Academic Press, Inc., and Harcourt Brace Jovanovich, New York, 1992), pp. 301–304.

[20] R. C. Stoneman, D. S. Thomson, and T. F. Gallagher, Phys. Rev. A **37**, 1527 (1988).

[21] M. Murakami and S.-I. Chu, Phys. Rev. A **88**, 043428 (2013).

[22] S.-I. Chu and W. P. Reinhardt, Phys. Rev. Lett. **39**, 1195 (1977).

[23] A. Giusti-Suzor and P. Zoller, Phys. Rev. A **36**, 5178 (1987).